Backbending phenomenon in ^{48}Cr

Takeshi Tanaka*
Research Institute of Electrical Communication, Tohoku University, Sendai, 980-8577 Japan

Kazuo Iwasawa
Institute of Physics, University of Tsukuba, Tsukuba, Ibaraki, 305-8571 Japan

Fumihiko Sakata
Department of Mathematical Sciences, Ibaraki University, Mito, Ibaraki, 310-8512 Japan
(Received 21 April 1998)

A new mechanism for the backbending phenomenon in ^{48}Cr is discussed based on a careful analysis of the yrast band, where no level crossing of the single-particle orbits is expected. A newly developed numerical code for solving the self-consistent cranked Hartree-Fock-Bogoliubov (HFB) equation with a maximum overlap criterion is applied to ^{48}Cr, and various continuous cranked HFB solutions forming many rotational bands are obtained. By using the first derivative of the cranked HFB wave function with respect to the total angular momentum, and by comparing the Thouless-Valatin and the Inglis moments of inertia, it is pointed out that a fully self-consistent mean-field treatment, which properly takes into account the two-body residual interaction, is crucial in explaining cases of backbending phenomena that are not associated with a single-particle level crossing. [S0556-2813(98)00211-8]

PACS number(s): 21.60.Jz, 21.10.Re

I. INTRODUCTION

The basic mechanism of backbending phenomena, first observed in rare earth nuclei, has been thought to be a quasiparticle level crossing between an unoccupied high-j intruder orbit and the most high-lying occupied orbit, which causes an abrupt change in the moment of inertia of the collective rotation. The main approach for analyzing these phenomena has been based on the cranked Nilsson-Strutinsky model, which has also been successful in explaining the superdeformed band.

From the standpoint of the nuclear many-body problem, nevertheless, many interesting questions remain. To what extent does the uniform rotation caused by a breaking of rotational invariance of the mean field persist? How stable is the deformed mean field with respect to the configuration change? How do the nonadiabatic effects between the collective rotation and the single-particle motion manifest themselves? In exploring these questions, one must carefully analyze various cases such as those of excited rotational bands or rotational bands in light nuclei, etc., where the nonadiabatic effects are expected to play a more crucial role than in rare earth nuclei.

High-spin states in ^{48}Cr exhibit a ''good'' rotor up to spin $I^{\pi}=10^{+}$, after which the yrast band starts to backbend. Recently, this yrast band has been experimentally established up to spin $I^{\pi}=16^{+}$ [1]. According to Caurier *et al.* [2], who compared the shell model calculation with the cranked Hartree-Fock-Bogoliubov (HFB) calculation by applying the Gogny force, it turns out that the orbits in the $1f_{7/2}$ shell play a dominant role in reproducing the backbending phenomenon in the ^{48}Cr yrast band, and there are no intruder orbits in this shell region. On the other hand, Hamamoto showed numerically that the single-particle orbits among one subshell do not show any level crossing in the case of the collective rotation [3]. One may thus predict that the backbending phenomenon in ^{48}Cr has a different mechanism than that discussed for rare earth nuclei.

Aiming at understanding in detail how the rotational state changes as the system acquires an additional angular momentum and how the single-particle orbits are nonlinearly affected by the collective rotation, we have developed a new numerical code, based on the reference state method [4], for solving the self-consistent cranked HFB equation. In contrast with the conventional methods, our method gives a continuous solution of the cranked HFB equation with respect to the total angular momentum, and enables us to explore various global properties of the rotational band by numerically evaluating various differential quantities such as $d\beta/dI$ and $d\gamma/dI$. It also suggests to what extent the cranked HFB state remains stable by keeping its identity as the system rotates faster. The objective of this study is to explore the microscopic dynamics responsible for the band-crossing phenomena in the fp-shell nuclei by applying our code to ^{48}Cr, a typical medium-light nucleus exhibiting a backbending phenomenon.

II. METHOD FOR ANALYSIS OF STRUCTURE CHANGES IN ROTATIONAL BANDS

In this section, we discuss the necessary formulas and notations for analyzing structure changes in rotational bands. For the sake of simplicity, we will discuss them within the cranked HF rather than the cranked HFB formalism. Inclusion of the pairing correlations is straightforward.

*Present address: Institute for Particle and Nuclear Studies, HEARO, Tanashi, Tokyo, 188-8501 Japan.

The intrinsic state $|\phi(I)\rangle$ is obtained by solving the cranked HF equation given as

$$\delta\langle\phi(I)|\hat{H}-\omega\hat{J}_x|\phi(I)\rangle=0, \tag{1a}$$

$$\langle\phi(I)|\hat{J}_x|\phi(I)\rangle=I. \tag{1b}$$

In numerically solving this equation, the Lagrange multiplier ω is determined as a function of I through the condition in Eq. (1b). The functional form of ω with respect to I is expressed as

$$\omega(I)=\frac{d\mathcal{H}_{\rm rot}(I)}{dI}, \quad \mathcal{H}_{\rm rot}(I)\equiv\langle\phi(I)|\hat{H}|\phi(I)\rangle. \tag{2}$$

Using the *intrinsic Hamiltonian in a rotating frame called the Routhian* $\hat{R}(I)\equiv\hat{H}-\omega(I)\hat{J}_x$, Eq. (1a) is expressed as

$$\delta\langle\phi(I)|\hat{R}(I)|\phi(I)\rangle=0. \tag{3}$$

Since the intrinsic state $|\phi(I)\rangle$ is a *stationary state* satisfying Eq. (3), the intrinsic Hamiltonian in the rotating frame is generally expressed as

$$\begin{aligned}\hat{R}(I)&\equiv\hat{H}-\omega(I)\hat{J}_x\\&=\langle\phi(I)|\hat{R}(I)|\phi(I)\rangle+\sum_\mu\epsilon_\mu(I)\hat{c}^\dagger_\mu(I)\hat{c}_\mu(I)\\&\quad-\sum_m\epsilon_m(I)\hat{c}_m(I)\hat{c}^\dagger_m(I)+:\hat{R}(I):,\end{aligned} \tag{4}$$

where $\{\hat{c}^\dagger_\mu(I),\hat{c}_m(I)\}$ are the particle- and hole-creation operators in the *rotating frame*, satisfying

$$\hat{c}_\mu(I)|\phi(I)\rangle=\hat{c}^\dagger_m(I)|\phi(I)\rangle=0. \tag{5}$$

Here and hereafter, the hole states are denoted by $m,n,\ldots$, and the particle states by $\mu,\nu,\ldots$. The operator $:\hat{R}(I):$ stands for the two-body residual interaction terms consisting of normal-ordered four fermion operators in the rotating frame.

The total angular momentum $\hat{J}_x$ and the *collective angle operator* $\hat{\Theta}(I)$ defined by

$$i\frac{\partial}{\partial I}|\phi(I)\rangle=\hat{\Theta}(I)|\phi(I)\rangle \tag{6}$$

satisfy the following equations [5]:

$$\langle\phi(I)|[\hat{\Theta}(I),\hat{J}_x]|\phi(I)\rangle=i, \tag{7}$$

$$\delta\langle\phi(I)|[\hat{R}(I),i\hat{\Theta}(I)]-\frac{d\omega(I)}{dI}\hat{J}_x|\phi(I)\rangle=0. \tag{8}$$

Since $d\omega(I)/dI$ is an inverse of the *Thouless-Valatin moment of inertia at a given value I*, and is a second derivative of the expectation value of the Hamiltonian, the following relation holds:

$$\begin{aligned}\{\mathcal{J}_{\rm TV}(I)\}^{-1}&\equiv\frac{d\omega(I)}{dI}=\frac{d^2\mathcal{H}_{\rm rot}(I)}{dI^2}\\&=\langle\phi(I)|[[\hat{R}(I),i\hat{\Theta}(I)],i\hat{\Theta}(I)]|\phi(I)\rangle.\end{aligned} \tag{9}$$

The right-most side of the above equation gives a matrix element appearing in the random phase approximation (RPA). Since the value of $\omega(I)$ is numerically obtained in the self-consistent cranked HF calculation, and our code numerically determines $\omega(I)$ as a continuous function of I by maintaining the characteristic properties of the band, the inverse of $\mathcal{J}_{\rm TV}(I)$ is evaluated using the relation $d\omega(I)/dI$, without calculating the RPA equation [6]. From the Thouless-Valatin moment of inertia, one may extract detailed information on the backbending phenomena.

By neglecting the two-body residual interaction $:\hat{R}(I):$ in Eq. (4), Eq. (9) is known to be reducible to the Inglis formula

$$\mathcal{J}_{\rm Ing}(I)=2\sum_{\mu m}\frac{|J_{\mu m}(I)|^2}{\epsilon_\mu(I)-\epsilon_m(I)}, \tag{10}$$

where $J_{\mu m}(I)$ is the particle-hole components of $\hat{J}_x$ with respect to $|\phi(I)\rangle$:

$$\begin{aligned}\hat{J}_x&\equiv I+\sum_{\mu m}\{J_{\mu m}(I)\hat{c}^\dagger_\mu(I)\hat{c}_m(I)+\text{H.c.}\}\\&\quad+\sum_{\mu\nu}J_{\mu\nu}(I)\hat{c}^\dagger_\mu(I)\hat{c}_\nu(I)-\sum_{mn}J_{mn}(I)\hat{c}_n(I)\hat{c}^\dagger_m(I).\end{aligned} \tag{11}$$

An I dependence of the matrix elements $J_{\mu m}(I)$ indicates not only a microscopic structure change of the self-consistent mean field $|\phi(I)\rangle$, but also a change of the properties of the collective rotation, as the total angular momentum of the system increases.

Since the angular frequency $\omega(I)$ is related to the first derivative of the cranked HF state through Eq. (2), and since its I-dependent properties ought to be understood in terms of $d|\phi(I)\rangle/dI$, let us consider the cranked HF state $|\phi(I+\Delta I)\rangle$ with an angular momentum $I+\Delta I$, slightly different from I, satisfying

$$\delta\langle\phi(I+\Delta I)|\hat{H}-\omega(I+\Delta I)\hat{J}_x|\phi(I+\Delta I)\rangle=0, \tag{12a}$$

$$\langle\phi(I+\Delta I)|\hat{J}_x|\phi(I+\Delta I)\rangle=I+\Delta I. \tag{12b}$$

With the single-particle operators in the *rotating frame* $\{\hat{c}^\dagger_\mu(I),\hat{c}_m(I)\}$ obtained within the cranked HF equations (1a) and (1b), $|\phi(I+\Delta I)\rangle$ is represented by means of an anti-Hermitian one-body operator $\Delta\hat{F}(I)$,

$$|\phi(I+\Delta I)\rangle=e^{\Delta\hat{F}(I)}|\phi(I)\rangle, \tag{13}$$

$$\Delta\hat{F}(I)=\sum_{\mu m}\{\Delta f^I_{\mu m}\hat{c}^\dagger_\mu(I)\hat{c}_m(I)-\text{H.c.}\}.$$

A set of $\{\Delta f^I_{\mu m},\Delta f^{I*}_{\mu m}\}$ in Eq. (13) represents a new cranked HF state $|\phi(I+\Delta I)\rangle$ in the TDHF symplectic phase space [7–10] called the TDHF manifold [11,12].

To explore the structure change of the cranked HF state by means of that in the occupied single-particle wave functions, one may use a diagonal component of the density matrix

$$\rho^I_{mm}(\Delta I)\equiv\langle\phi(I+\Delta I)|\hat{c}^\dagger_m(I)\hat{c}_m(I)|\phi(I+\Delta I)\rangle, \quad (14)$$

which tells us to what extent the occupied single-particle state m defined at I undergoes a change when the system acquires additional small angular momentum ΔI. With the aid of $\Delta f^I_{\mu m}$ defined in Eq. (13), $\rho^I_{mm}(\Delta I)$ is expressed as

$$\rho^I_{mm}(\Delta I)=(\cos^2\sqrt{\Delta\boldsymbol{f}^\dagger(I)\Delta\boldsymbol{f}(I)})_{mm}, \quad [\Delta\boldsymbol{f}(I)]_{\mu m}=\Delta f^I_{\mu m}. \quad (15)$$

Expanding $\rho^I_{mm}(\Delta I)$ up to the second order in $\Delta f^I_{\mu m}$, one gets

$$\rho^I_{mm}(\Delta I)\approx 1-\sum_\mu \Delta f^{I*}_{\mu m}\Delta f^I_{\mu m}+\cdots. \quad (16)$$

As is understood from Eq. (16), the amount of decrease from the unit value in the diagonal component $\rho^I_{mm}(\Delta I)$ depends on how much the occupied state m at I is rearranged by taking account of the unoccupied components μ at I, as the system acquires an additional angular momentum ΔI. This rearrangement in the single-particle states tells us how much the self-consistent mean field is altered by an increase of the total angular momentum.

Dividing the *local* quantities $\rho^I_{mm}(\Delta I)$ by the infinitesimal additional angular momentum ΔI, one may thus introduce a new quantity $\mathcal{O}_m(I)$

$$\mathcal{O}_m(I)\equiv\sqrt{\lim_{\Delta I\to 0}\frac{1-\rho^I_{mm}(\Delta I)}{(\Delta I)^2}}, \quad (17)$$

which represents how much each occupied orbit m changes at a given angular momentum I. Using Eq. (16), one may represent $\mathcal{O}_m(I)$ as

$$[\mathcal{O}_m(I)]^2\approx\frac{[\Delta\boldsymbol{f}^\dagger(I)\Delta\boldsymbol{f}(I)]_{mm}}{(\Delta I)^2}=\sum_\mu \frac{\Delta f^{I*}_{\mu m}}{\Delta I}\frac{\Delta f^I_{\mu m}}{\Delta I}. \quad (18)$$

Let us consider the relation between $\mathcal{O}_m(I)$ and the moment of inertia $\mathcal{J}_{\rm TV}(I)$. Using a perturbative expansion of the cranked HF equations (12a) and (13) with respect to ΔI and $\Delta f^I_{\mu m}$ (the latter quantities are considered to be of the same order as the former), one may obtain the first-order equation for determining $\Delta f^I_{\mu m}$ as[1]

$$[\epsilon_\mu(I)-\epsilon_m(I)]\Delta f^I_{\mu m}+\sum_{\nu n}\{\Delta f^I_{\nu n}\mathcal{A}(\nu n;m\mu;I)+\Delta f^{I*}_{\nu n}\mathcal{B}(n\nu;m\mu;I)\}=\Delta\omega J_{\mu m}(I), \quad (19)$$

where $\mathcal{A}(\nu n;m\mu;I)$ and $\mathcal{B}(n\nu;m\mu;I)$ are the two-body matrix elements of $:\hat{R}(I):$ defined by

$$\mathcal{A}(\nu n;m\mu;I)\equiv-\langle\phi(I)|[[:\hat{R}(I):,\hat{c}^\dagger_\nu(I)\hat{c}_n(I)],\hat{c}^\dagger_m(I)\hat{c}_\mu(I)]|\phi(I)\rangle, \quad (20)$$

$$\mathcal{B}(n\nu;m\mu;I)\equiv\langle\phi(I)|[[:\hat{R}(I):,\hat{c}^\dagger_n(I)\hat{c}_\nu(I)],\hat{c}^\dagger_m(I)\hat{c}_\mu(I)]|\phi(I)\rangle,$$

and $\Delta\omega$ is an additional rotational frequency

$$\Delta\omega\equiv\omega(I+\Delta I)-\omega(I)=\frac{\partial^2\mathcal{H}_{\rm rot}(I)}{\partial I^2}\cdot\Delta I+O[(\Delta I)^2]. \quad (21)$$

These equations are well-known relations in the RPA. Dividing both sides of Eq. (19) by ΔI, and replacing $\Delta\omega/\Delta I$ with $\{\mathcal{J}_{\rm TV}(I)\}^{-1}$, one may obtain

$$[\epsilon_\mu(I)-\epsilon_m(I)]\frac{\Delta f^I_{\mu m}}{\Delta I}+\sum_{\nu n}\left\{\frac{\Delta f^I_{\nu n}}{\Delta I}\mathcal{A}(\nu n;m\mu;I)+\frac{\Delta f^{I*}_{\nu n}}{\Delta I}\mathcal{B}(n\nu;m\mu;I)\right\}=\frac{J_{\mu m}(I)}{\mathcal{J}_{\rm TV}(I)}. \quad (22)$$

Equation (22) shows that $\mathcal{O}_m(I)$ are related with the Thouless-Valatin moment of inertia and the two-body residual interaction.

---

[1]The expectation value of the Routhian $\langle\phi(I+\Delta I)|\hat{R}(I+\Delta I)|\phi(I+\Delta I)\rangle$ is expanded as

$$\begin{aligned}&\langle\phi(I+\Delta I)|\hat{R}(I+\Delta I)|\phi(I+\Delta I)\rangle\\&=\langle\phi(I+\Delta I)|\hat{R}(I)-\Delta\omega\hat{J}_x|\phi(I+\Delta I)\rangle\\&=\langle\phi(I)|\hat{R}(I)|\phi(I)\rangle-\Delta\omega\langle\phi(I)|\hat{J}_x|\phi(I)\rangle\\&\quad+\langle\phi(I)|[\hat{R}(I),\Delta\hat{F}(I)]|\phi(I)\rangle-\Delta\omega\langle\phi(I)|[\hat{J}_x,\Delta\hat{F}(I)]|\phi(I)\rangle\\&\quad+\tfrac{1}{2}\langle\phi(I)|[[\hat{R}(I),\Delta\hat{F}(I)],\Delta\hat{F}(I)]|\phi(I)\rangle+\cdots.\end{aligned}$$

Differentiating both sides of Eq. (26) by $\Delta f^{I*}_{\mu m}$, and using the cranked HF conditions (1a) and (12a), one may obtain Eq. (19).

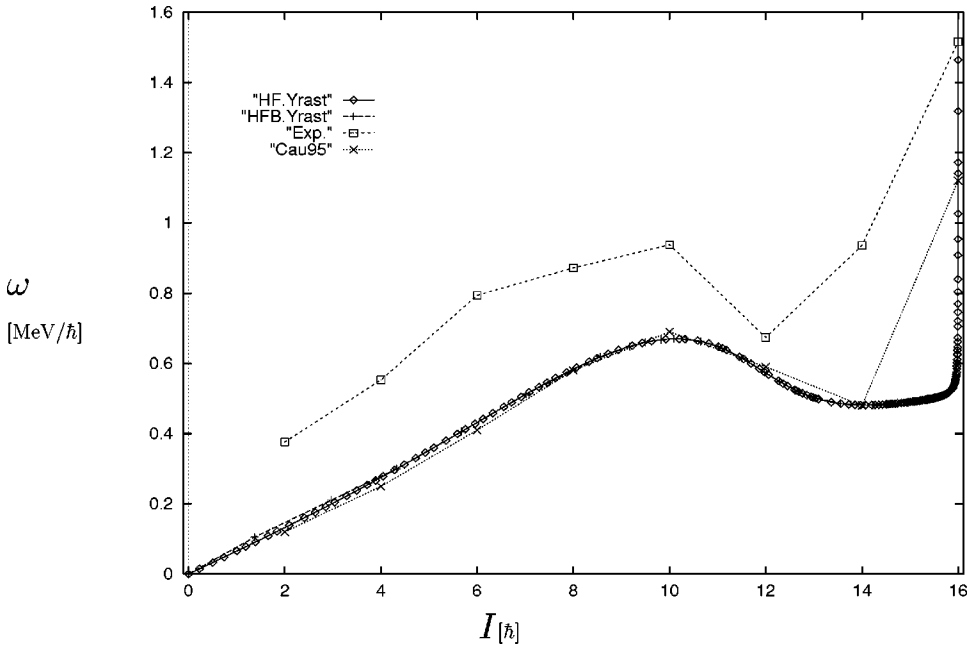

FIG. 1. Lagrange multipliers ω in the cranked HF and cranked HFB calculations versus the angular momentum I. The experimental data from Ref. [1] and values from the cranked HFB calculations in Ref. [2] are denoted by Exp. and Cau95, respectively.

Evaluating $\mathcal{O}_m(I)$, one may estimate how much the structure of the occupied single-particle states changes depending on I, i.e., how much the system must adjust its self-consistent mean field to accommodate the faster rotation. By the use of the microscopic quantities $\mathcal{O}_m(I)$, one may extract the nonadiabatic effects between the collective rotational motion and the single-particle motion. This proves useful when investigating backbending phenomena that are not accompanied by a single-particle level-crossing, as we discuss in the next section.

III. NUMERICAL CALCULATIONS

A. Conventional mechanism of backbending phenomena

To investigate the microscopic dynamics responsible for the backbending phenomenon in ^{48}Cr, we have performed numerical calculations for both the cranked HF and cranked HFB equations with Gogny D1 force [13–15], using the reference state method [4], which automatically gives the solution as a continuous function of the total angular momentum I. As the convergence condition for each cranked HF state, we impose

$$\frac{1}{A}\sqrt{\sum_{m=\mathrm{occ}}(\langle m(I)^{(n)}|\boldsymbol{R}^{(n)}_{\text{one-body}}(I)^2|m(I)^{(n)}\rangle-\langle m(I)^{(n)}|\boldsymbol{R}^{(n)}_{\text{one-body}}(I)|m(I)^{(n)}\rangle^2)}\leqslant 10[\mathrm{eV}], \tag{23}$$

where $|m(I)^{(n)}\rangle$ denotes a single-particle state appearing at the nth iteration in the course of solving the cranked HF equation, and $\boldsymbol{R}^{(n)}_{\text{one-body}}(I)$ is a one-body Routhian matrix folded by a density matrix defined at the nth iteration,

$$\rho^{(n)}_{\alpha\beta}(I)\equiv\sum_{m=\mathrm{occ}}\langle\beta|m(I)^{(n)}\rangle\langle m(I)^{(n)}|\alpha\rangle. \tag{24}$$

TABLE I. Total Binding Energies of the ground and $2p$-$2h$ states at $\omega=0$. The experimental value is cited from Ref. [19].

	HFB	HF	Exp.
Ground state [MeV]	−409.386	−409.347	−411.462
$2p$-$2h$ state [MeV]	−404.790	−404.792	

In the HFB calculation, a similar convergence condition is employed.

Since the ground state of ^{48}Cr has an axial symmetric shape [2], the z axis is chosen as the symmetry axis. Our code includes the major shells up to the principle quantum number $N=6$, and imposes parity and signature symmetry.[2] For the maximum overlap criterion required by the reference state method [4], our code required that the overlap between two neighboring cranked HF(B) states in the same band,

[2]In our numerical calculations, the single-particle wave functions are expressed in an expanded form using three-dimensional harmonic oscillator bases with a fixed range parameter, which is defined so as to reproduce the largest binding energy of the ground state.

having the total angular momenta I and $I+\Delta I$, should be more than 0.9. That is to say, each small increment ΔI is numerically adjusted by the maximum overlap criterion, so as to maintain the identity of the band.[3] Unlike the conventional methods, our numerical calculation using the reference state method can evaluate quantities such as $d\beta/dI$, $d\gamma/dI$, and $\mathcal{O}_m(I)$, since the cranked HF(B) states connected by the maximum overlap criterion may be regarded both as belonging to the same band, and as an analytic function of the total angular momentum I.

Our numerical calculations have demonstrated that the Gogny-D1 force reproduces well the binding energy of the ground state both in the HF and HFB calculations (Table I). Although our calculated values for the rotational energies do not agree well with their absolute values from experimental data [1,2], our numerical results do reproduce well the results of the cranked HFB calculations in Ref. [2] where a much wider shell space was applied than in our present calculations (Fig. 1).

As is seen in Fig. 1, the Lagrange multiplier $\omega(I)$ of the yrast band first increases in the region $0\hbar \lesssim I \lesssim 10\hbar$, then decreases in $10\hbar \lesssim I \lesssim 14\hbar$. $\omega(I)$ begins to increase again at $I \sim 14\hbar$, and then diverges at $I=16\hbar$, where the full alignment of all particles in the fp shell is completed, terminating the yrast band built upon the ground state [16].

After obtaining the ground state ($I=0\hbar$ state in the yrast band), one may construct a $1p$-$1h$ state composed of the most low-lying unoccupied orbit and the most high-lying occupied orbit within the parity $\pi=-$ and signature $\alpha=+$ subspace of the single-particle Routhian. Taking the thus-constructed $1p$-$1h$ state as a trial function for the cranked HFB equation, one may obtain an excited HF(B) state upon convergence of the iterative calculation. In order to reach the HF(B) state, which has the largest overlap with the initial trial wave function and is thus characterized by a relative configuration with respect to the yrast band, one has to use the reference state method [4]. In this way, the three different excited HF(B) states shown in Fig. 2 are obtained by starting with the neutron $1p$-$1h$ state, the proton $1p$-$1h$ state, and the $2p$-$2h$ state where both the proton and neutron $1p$-$1h$ are excited simultaneously.

Starting from the thus-obtained excited HF(B) states, the excited rotational bands satisfying the maximum overlap criterion have been calculated up to their termination points. The neutron and proton $1p$-$1h$ excited bands terminate at $I=14\hbar$, and the $2p$-$2h$ excited band at $I=12\hbar$.

It is worth mentioning that the $2p$-$2h$ excited band shows a small triangle shape in $E-I$ plot near the backbending region of the yrast band, as has been pointed out in respect to medium-heavy nuclei both by Hamamoto [3] and Marshalek and Goodman [17]. It should also be mentioned that our numerical calculation does not necessarily give a continuous solution up to the band termination point, since either the convergence condition or the maximum overlap criterion may eventually prevent us from proceeding to a higher angular momentum region. These points are related to the stability of the cranked HF solution, and will be discussed extensively in a forthcoming paper.

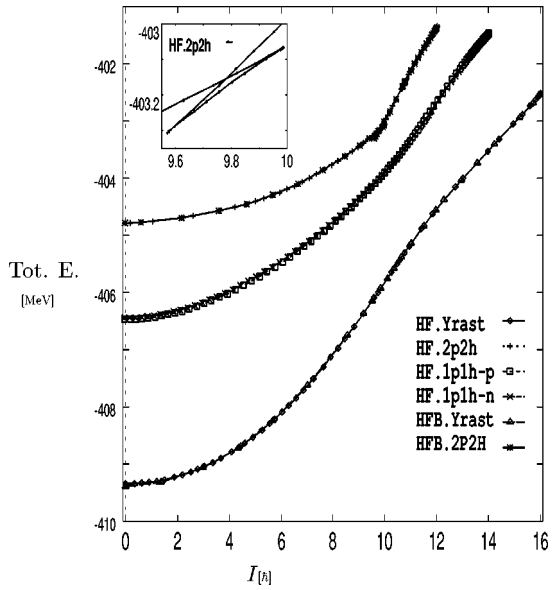

FIG. 2. Total binding energies for the yrast, neutron $1p$-$1h$, proton $1p$-$1h$, and $2h$-$2h$ rotational bands. The triangle shape of the $2h$-$2h$ band is shown in the upper left.

According to Hamamoto [3] and Marshalek and Goodman [17], the cranking calculation in medium-heavy nuclei shows a large angular momentum fluctuation in the backbending region. This is known to be caused by an unphysical mixing between two bands with different angular momenta, and to be a fatal defect of the cranked HFB treatment where the coupling between two bands with different angular momenta is incorrectly evaluated at a given angular frequency ω. This unphysical coupling causes a large variance of the total angular momentum defined by

$$\Gamma(I)=\sqrt{\langle\phi(I)|\hat{J}_x^2|\phi(I)\rangle-\langle\phi(I)|\hat{J}_x|\phi(I)\rangle^2}, \qquad (25)$$

in the backbending region. In our cranked HF and cranked HFB calculations for ^{48}Cr, however, there was no large fluctuation of I, as is shown in Fig. 3. This fact indicates that the backbending in ^{48}Cr is not caused by a strong mixing between two bands having different total angular momenta. It may also be observed in Fig. 2 that no band crossing is apparent in the backbending region.

As was discussed by Sorensen [18], who examined the above-mentioned point raised by Hamamoto, the backbending phenomena in medium-heavy nuclei are well described by the self-consistent HFB formalism, provided the BCS treatment of the pairing correlation is accurate enough and the quasiparticles are defined in a fully self-consistent way. In our present calculation, however, the binding energies obtained within the cranked HF calculation show a remarkable agreement with those obtained within the cranked HFB calculation for both the yrast and the $2p$-$2h$ bands, as seen in Fig. 2. This agreement is due to the fact that the pairing force contributes to the binding energy very weakly in this nucleus. Since the pairing gap disappears as a result of the Coriolis antipairing effects at $I \approx 4\hbar$ in the yrast band, and is mostly negligible in the $2p$-$2h$ band, the pairing correlation

[3]In the backbending region, we impose a stricter condition to obtain more precise information.

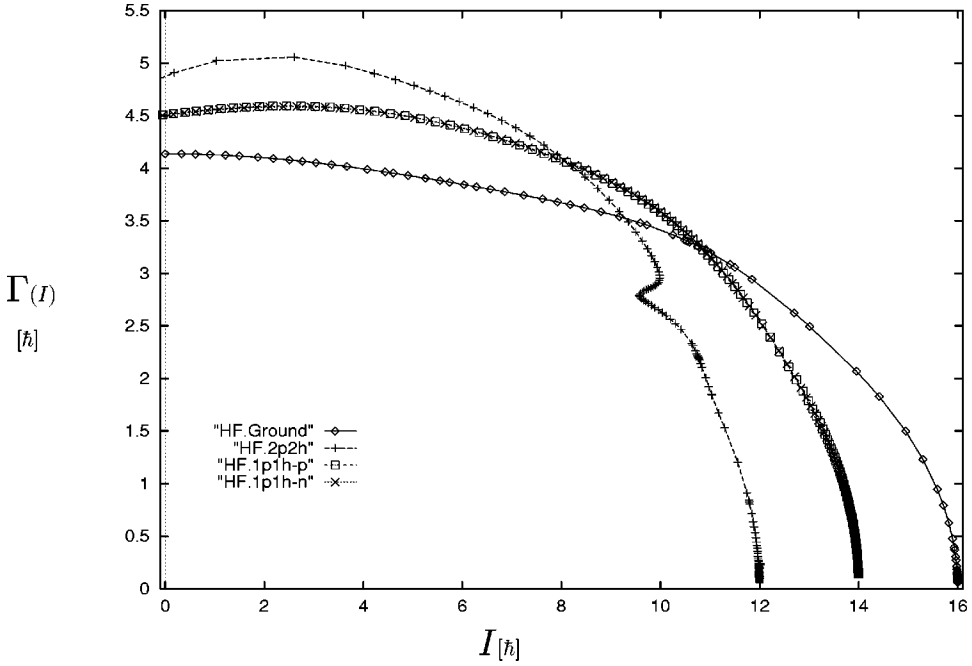

FIG. 3. Fluctuation of total angular momentum $\Gamma(I)$.

does not play any important role in the backbending phenomenon in ^{48}Cr. This suggests that the mechanism of the backbending phenomenon in ^{48}Cr may differ from those in medium-heavy and rare earth nuclei.

We end this subsection by briefly discussing the conventional analysis of the geometrical properties of the yrast band. In Fig. 4(a), the yrast band solution of the cranked HFB equation is presented in the $\beta-\gamma$ plane. The yrast band has an axial symmetric prolate shape up to $I=8$. An asymmetric deformation with negative γ starts to occur at $I=8$, then monotonically increases until $I=14$. After that, the system tends to reach the $\gamma=\pi/3$[rad.] oblate shape with a small β deformation at $I=16$, where the yrast band terminates. This geometrical structure change is usually attributed to a property change from the collective rotation to the noncollective rotation, which generates the total angular momentum. However, it is difficult to investigate based on Fig. 4(a) what happens in the intrinsic state, or why the backbending is induced through the asymmetric deformation.

In order to more clearly understand the microscopic mechanism of backbending phenomena in medium-light nuclei, the derivatives $d\beta/dI$ and $d\gamma/dI$ are numerically evaluated as shown in Fig. 4(b). It should be noted that these quantities are crucial to an understanding of the backbending phenomena, since the angular frequency $\omega(I)$ is related to the first derivative of the total Hamiltonian $\mathcal{H}_{\rm rot}(I)$ with respect to the total angular momentum I given by Eq. (2). As may be clearly recognized from this figure, the properties of the yrast band start to change at $I=6$, and the most dramatic change occurs at $I=12$. Since the structure change of the intrinsic state exhibited by the shape parameters β and γ is a net effect coming from many occupied single-particle orbits, it is desirable to explore the interrelation between the collective rotation (macrolevel dynamics) and the individual single-particle motion (microlevel dynamics) in a more comprehensive manner by employing the quantities $\mathcal{O}_m(I)$ introduced in the previous section.

B. New mechanism for backbending phenomenon in ^{48}Cr

We are now in a position to discuss a new mechanism for the backbending phenomenon in ^{48}Cr. Since our numerical calculations show that the effect of the pairing force in ^{48}Cr is negligibly small, we hereafter concentrate on the results of the cranked HF calculation. As ^{48}Cr is a $Z=N$ nucleus consisting of 24 protons and 24 neutrons, the proton field and the neutron field in the yrast band are expected to show very symmetric behavior. Figure 5 clearly shows that the proton and neutron single-particle Routhians along the yrast band exhibit very similar behavior, even though their absolute values are different. Also, as seen in Fig. 2, the excitation energies of the excited rotational bands characterized by the neutron $1p$-$1h$ configuration nearly coincide with those of the proton $1p$-$1h$ configuration. Because of this symmetry, we may hereafter confine our discussion to the single-particle orbits of the neutron field. Our numerical calculations indicate that the lower shells with $N=1$ and 2 can be regarded as the core. Hence we will only pay attention to the behaviors of the single-particle orbits near the $1f_{7/2}$ shell in the neutron field. It should be noted that these orbits are not pure $1f_{7/2}$ orbits since they are affected by other subshells in the fp shell due to the deformation of the system.

For the axial symmetric ground state, the single-particle wave functions are specified by the quantum number Ω of $\hat{J}_z$. In Fig. 5(a), which shows the single-particle Routhians along the yrast band, there are two orbits near $I=0\hbar$ and just below the Fermi surface, which are mainly described by the linear combination of two eigenfunctions with $\Omega=\pm 3/2\hbar$. Below these, there is another pair of orbits whose main components are the eigenfunctions with $\Omega=\pm 1/2\hbar$. At $I\approx 0\hbar$, these two pairs of orbits interact strongly with each other due to the cranking term, but hardly with the unoccupied orbits. Increasing the Lagrange multiplier ω, one finds that the pair of orbits starting with $\Omega=\pm 1/2\hbar$ at $I=0\hbar$ aligns rapidly, as shown in Fig. 6, and that these orbits are hardly affected by

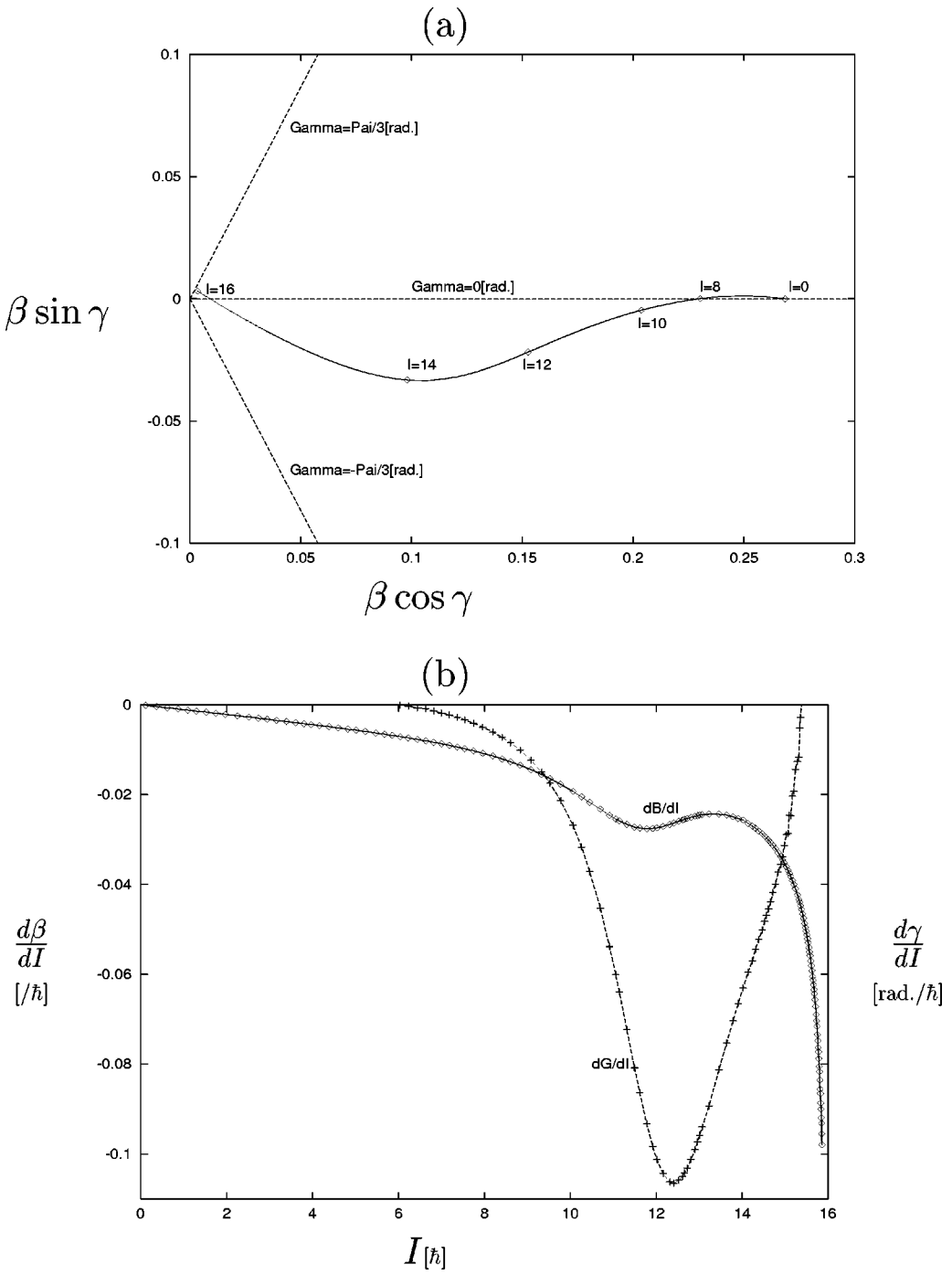

FIG. 4. Degree of structure change in $\beta-\gamma$ plane. (a) $\beta-\gamma$ plot of the yrast band, (b) $d\beta/dI$ (solid line with diamonds) and $d\gamma/dI$ (broken line with crosses).

the unoccupied orbits. In other words, the alignment of the orbits starting with $\Omega=\pm 1/2\hbar$ is mainly responsible for the increase of the total angular momentum in the low-I region. By comparison, the alignment of the orbits starting with $\Omega=\pm 3/2\hbar$ contributes much less to the total angular momentum in this region. In particular, the most high-lying occupied orbit with $\pi=-$ and $\alpha=+$, hereafter denoted by m^*, even shows an antialigning character, and so contributes negatively to the total angular momentum up to $I\approx 8\hbar$.

The particle-hole components $J_{\mu m}(I)$ are known to provide important information regarding the microscopic structure of the collective rotation at I, and the value of $\Gamma(I)$ represents the degree to which the rotational symmetry of the system is violated. As Fig. 7 shows, the matrix elements $J_{\mu m}(I)$ between the most high-lying occupied orbits starting with $\Omega=\pm 3/2\hbar$ at $I=0\hbar$ and the most low-lying unoccupied orbits starting with $\Omega=\pm 5/2\hbar$ have large values. One may thus infer that the fluctuation $\Gamma(I)$ is caused mainly by these matrix elements. Since $\hat{J}_x$ satisfies the weak commutation relation (7), which characterizes the local microscopic structure of the collective rotation together with Eq. (8), one may state that the occupied orbits from $\Omega=\pm 3/2\hbar$ and the

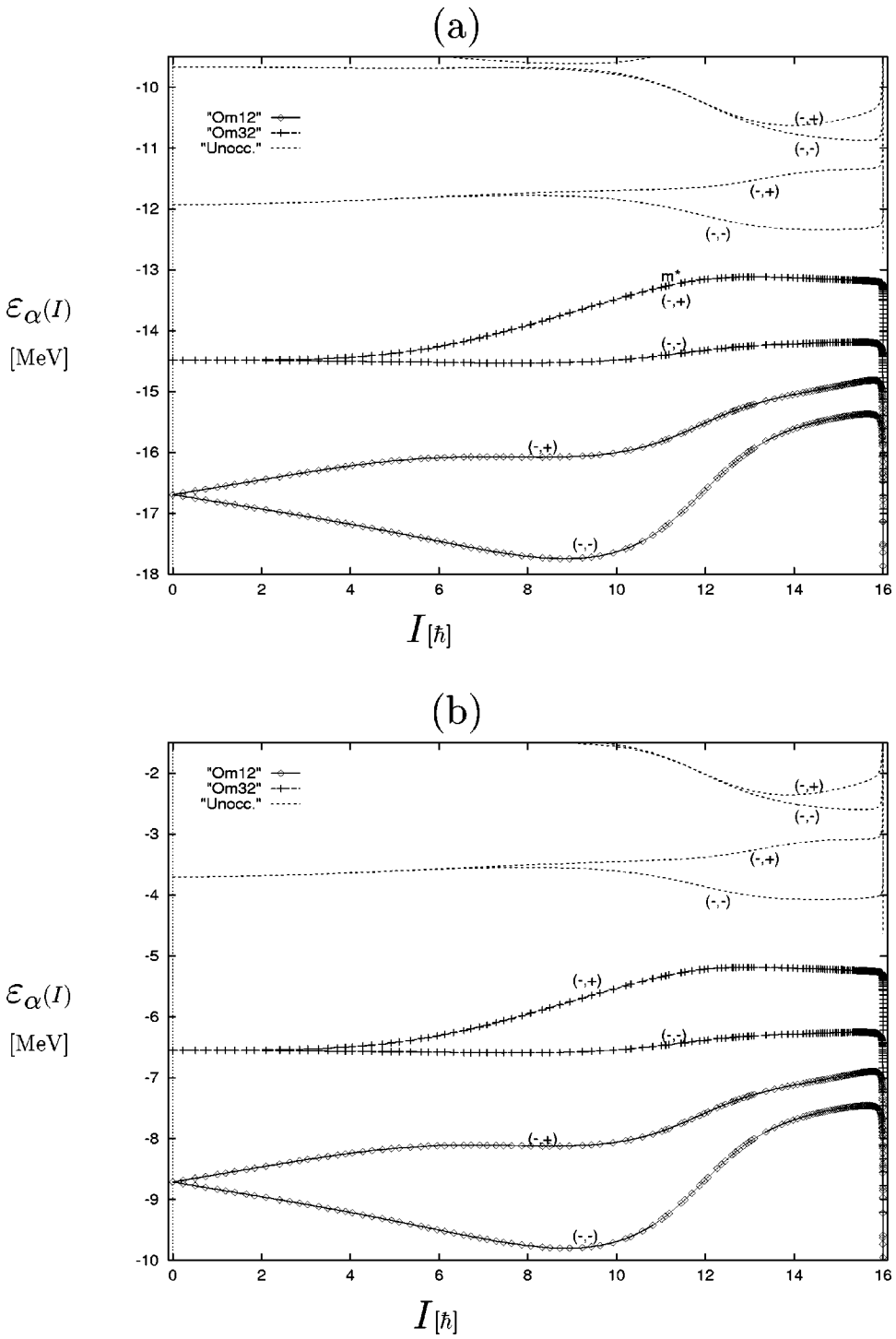

FIG. 5. Neutron (a) and proton (b) single-particle Routhians $\varepsilon_\alpha(I)$ along the yrast band near the Fermi surface. Om12 (solid lines with diamonds) and Om32 (broken lines with crosses) stand for the occupied orbits starting with $\Omega=\pm 1/2$ and with $\Omega=\pm 3/2$ at $I=0$, respectively. Unoccupied orbits are denoted by Unocc. (dashed lines). (π,α) denotes the parity and signature.

unoccupied orbits from $\Omega=\pm 5/2\hbar$ are also mainly responsible for generating the collective rotation up to $I\approx 8\hbar$, as is clearly seen in Figs. 6 and 7.

Beginning at $I\approx 8\hbar$, one can see the onset of a different mechanism that generates the additional total angular momentum. As Fig. 6 shows, the expectation values $J_{mm}(I)$ of the occupied orbits starting from $\Omega=\pm 1/2\hbar$ begin to saturate at around $I=8\hbar$, so that the alignment of these orbits can no longer remain a main resource for increasing the total angular momentum I. Therefore, the increase of I from this point could be seen as being mainly due to the alignment of the orbits starting from $\Omega=\pm 3/2\hbar$. As we have remarked previously, the most high-lying occupied orbit m^* shows an antialigning character before $I\approx 8\hbar$, and begins to align thereafter, whereas the other occupied orbits always show an aligning character. This fact implies that the degrees of freedom associated with m^* play the major role in reproducing the backbending phenomenon. When one compares Fig. 2

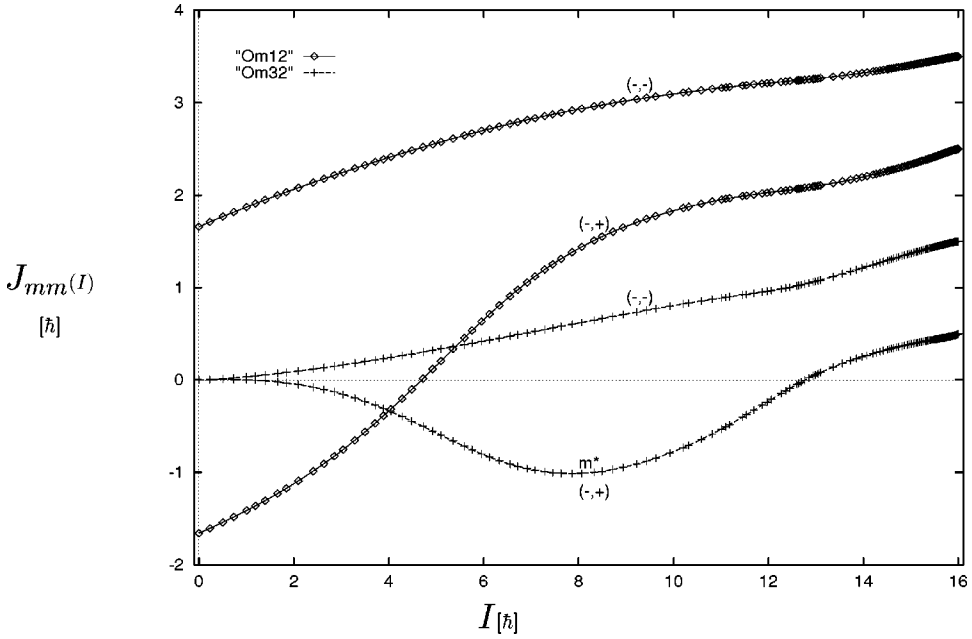

FIG. 6. Diagonal matrix elements of the total angular momentum $J_{mm}(I)$ for neutron occupied orbits along the yrast band. Om12 and Om32 are the same as in Fig. 5.

with Fig. 6, it becomes clear that the backbending phenomenon in ^{48}Cr is induced by a change in the microscopic mechanism that creates the angular momentum, and is thus mainly caused by one specific occupied orbit m^*.

The properties of the collective rotation should also be affected by the alignment of the orbits from $\Omega = \pm 3/2\hbar$, which play the major role in generating the collective rotation before $I \approx 8\hbar$. As Fig. 7 shows, the two largest values of $|J_{\mu m}(I)|^2$ have different I dependences after $I \approx 12\hbar$, whereas the third largest reaches its maximum value at $I \approx 8\hbar$, and then forms a trough at $I \approx 9\hbar$. These facts clearly show that the microscopic structure of the collective rotation does change at around $I \approx 8\hbar$ and $I \approx 12\hbar$. It should be mentioned that the I dependence of $J_{\mu m}(I)$ in Fig. 7 also provides important information regarding how the self-consistent mean field is rearranged, as the total angular momentum of the system increases. It should also be noted that no single-particle level crossing occurs between the occupied orbit m^* and the most low-lying unoccupied orbit within the space where $\pi = -$ and $\alpha = +$, as seen in Fig. 5.

In order to more closely investigate the important role of the orbit m^* in reproducing the backbending phenomenon, let us study the quantities $\mathcal{O}_m(I)$ defined in Sec. II. As Fig. 8 shows, the degree of structure change of the occupied orbits

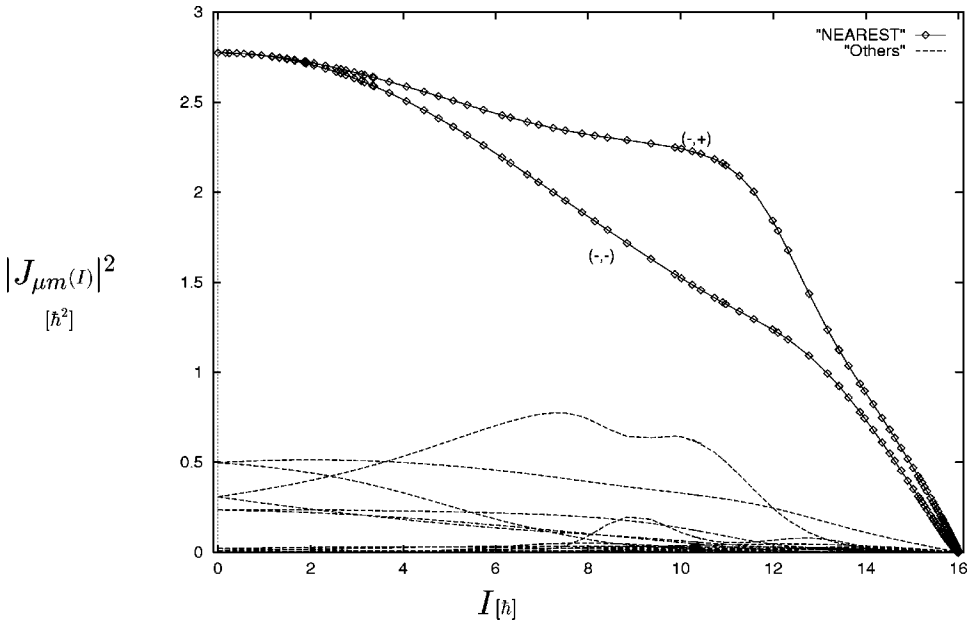

FIG. 7. Particle-hole matrix elements of the total angular momentum $\{J_{\mu m}(I)\}$ within the negative parity neutron single-particle states. Nearest (solid lines with diamonds) denotes the matrix element between two orbits having the same signature, which are located just above and just below the Fermi surface for that signature. Matrix elements between other orbits in the fp shell are denoted by others (broken lines).

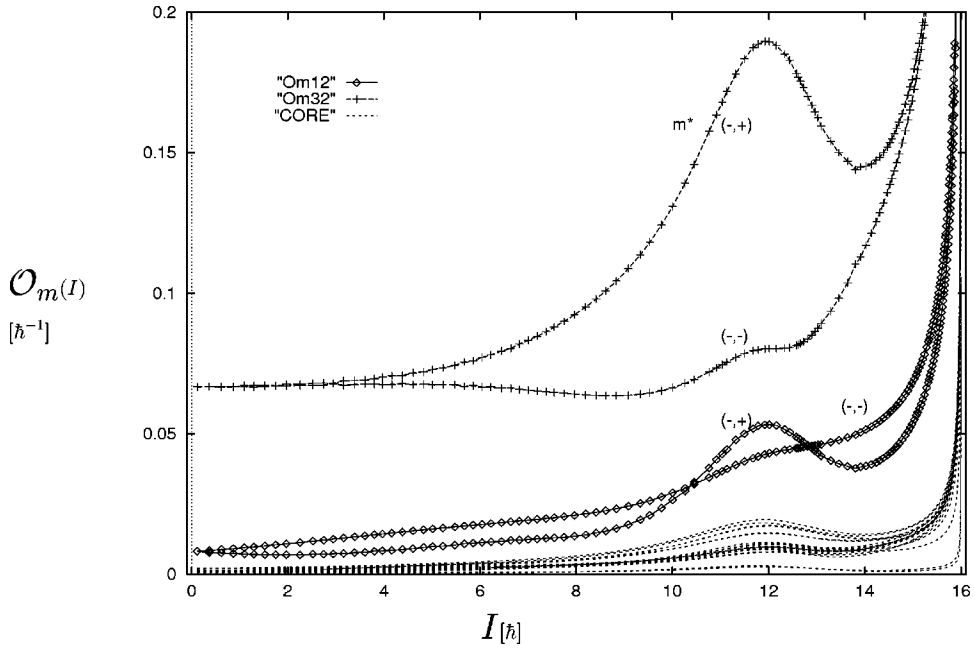

FIG. 8. Degree of structure change in the occupied orbits $\mathcal{O}_m(I)$ along the yrast band. Om12 and Om32 are the same as in Fig. 5. Core (broken lines) denotes the occupied orbits in the major shells with $N=1$ or 2.

is almost constant up to $I\approx 6\hbar$. By contrast, the degree of structure change for m^*, given by $\mathcal{O}_{m^*}(I)$, begins to increase at $I\approx 6\hbar$, although that of its signature partner orbit remains unchanged. $\mathcal{O}_{m^*}(I)$ increases rapidly, showing a local maximum at $I\approx 12\hbar$, then decreases until $I\approx 14\hbar$. In other words, the microscopic structure of the most high-lying occupied orbit m^* changes most at $I\approx 12\hbar$. As we have pointed out in reference to Fig. 6, the contribution of m^* to the total angular momentum changes from negative (antialigning) to positive (aligning) as the alignment of the occupied orbits originating from $\Omega=\pm 1/2\hbar$ brings their expectation values close to saturation. We have also discussed, in reference to Fig. 4(b), that the system starts to deform toward the γ direction after $I\approx 8\hbar$. From these numerical results, one may extract the following microscopic dynamics: the system has to change its shape self-consistently so as to create an occupied orbit, such as m^*, that is able to align toward the direction of the total angular momentum after the simple alignment mechanism due to the one-body Coriolis term has terminated.

As we stated in the previous subsection, the angular frequency $\omega(I)$ is expressed by the derivative of the total Hamiltonian $\mathcal{H}_{\rm rot}(I)$ with respect to I given in Eq. (2). Since the I dependence of $\mathcal{H}_{\rm rot}(I)$ is coming from that of the cranked HF state $|\phi(I)\rangle$, the property change of $\omega(I)$ is directly related to the first derivative of the cranked HF state with respect to I. Comparing Figs. 4 and 8, one may easily find a similar I dependence between $\mathcal{O}_{m^*}(I)$ and the first derivatives of the shape parameters $d\beta/dI$ and $d\gamma/dI$. The latter quantities reach the local minimum at $I\approx 12$, reflecting the large degree of structure change in the cranked HF state evaluated by $d|\phi(I)\rangle/dI$. It should be pointed out that these quantities express a net effect from various single-particle states, whereas $\mathcal{O}_m(I)$ represents an individual effect coming from m. From Figs. 4 and 8, however, one may draw the important conclusion that the geometrical structure change of the cranked HF state in the β-γ plane is mainly caused by only one occupied orbit m^*, and its importance is due to the large value of $\mathcal{O}_{m^*}(I)$.

Before we discuss the microscopic mechanism that creates the special occupied orbit m^*, let us briefly consider why all the components of $\mathcal{O}_m(I)$ diverge in the high spin region $I\geqslant 14\hbar$, as is shown in Fig. 8, in which the occupied orbits become completely aligned. Using the variational parameter $\Delta f^I_{\mu m}$ defined in Eq. (13) and the matrix element $J_{\mu m}(I)$, one may approximate the infinitesimal angular momentum ΔI as

$$\Delta I\approx\sum_{\mu m}\ (J_{\mu m}(I)\Delta f^{I*}_{\mu m}+\text{H.c.}). \tag{26}$$

Dividing both sides of Eq. (26) by ΔI, one obtains

$$1\approx\sum_{\mu m}\left(J_{\mu m}(I)\frac{\Delta f^{I*}_{\mu m}}{\Delta I}+\text{H.c.}\right). \tag{27}$$

Since all ph components of $J_{\mu m}(I)$ vanish at the band terminating point [16], the quantities $\{\Delta f^I_{\mu m}/\Delta I\}$, i.e., $\mathcal{O}_m(I)$, diverge so as to satisfy Eq. (27).

Let us discuss now the microscopic mechanism of the backbending phenomenon in ^{48}Cr by exploiting numerical results for the moment of inertia. According to Eq. (9), one may explore the backbending phenomenon in detail through $\{\mathcal{J}_{\rm TV}(I)\}^{-1}$, whose numerical values are shown in Fig. 9. By comparing Figs. 8 and 9, one may recognize that the quantity $\{\mathcal{J}_{\rm TV}(I)\}^{-1}$, similar to $d\beta/dI$ and $d\gamma/dI$, shows an I dependence that is similar to that of $\mathcal{O}_{m^*}(I)$, which as we have seen suggests the basic role of the occupied orbit m^* in producing the backbending phenomenon in ^{48}Cr. This coincidence is not accidental, since $\mathcal{O}_{m^*}(I)$ and $\{\mathcal{J}_{\rm TV}(I)\}^{-1}$ are related to each other through Eq. (22).

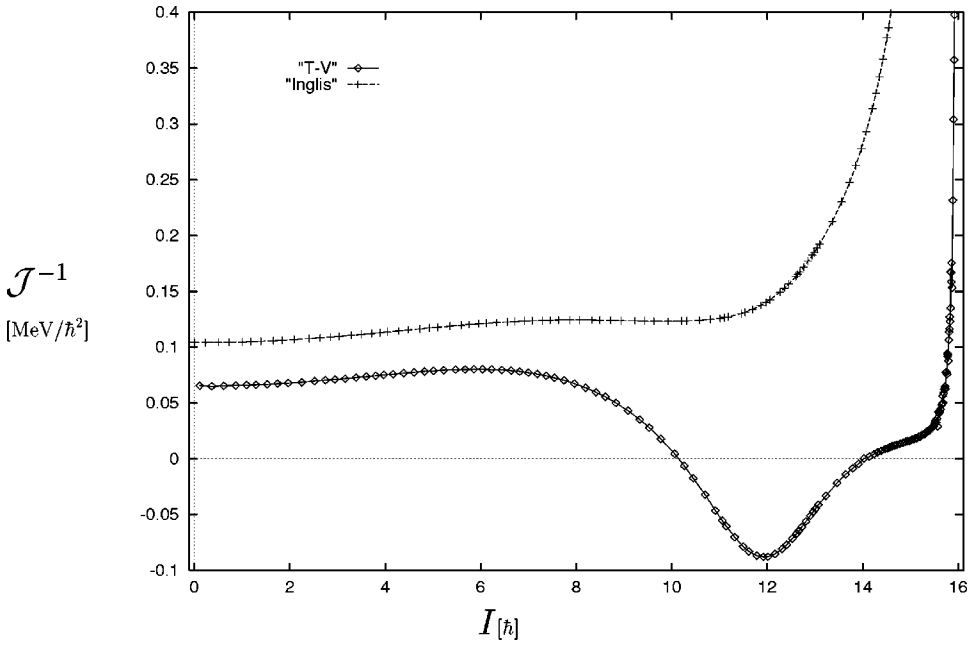

FIG. 9. Inverse of the moment of inertia of the yrast band. T-V (solid line with diamonds) and Inglis (broken line with crosses) denote $\{\mathcal{J}_{\mathrm{TV}}(I)\}^{-1}$ and $\{\mathcal{J}_{\mathrm{Ing}}(I)\}^{-1}$, respectively.

Figure 9 also depicts the numerical values of $\mathcal{J}_{\mathrm{Ing}}(I)$. In spite of their differences in absolute value, our numerical results for both $\mathcal{J}_{\mathrm{TV}}(I)$ and $\mathcal{J}_{\mathrm{Ing}}(I)$ show a very similar I dependence up to $I \approx 6\hbar$: in fact, they are almost constant up to that point. At $I \approx 8\hbar$, however, $\{\mathcal{J}_{\mathrm{TV}}(I)\}^{-1}$ starts to decrease, reaching a minimum value at $I \approx 12\hbar$, whereas $\mathcal{J}_{\mathrm{Ing}}(I)$ remains almost unchanged up to $I \approx 12\hbar$. Both diverge at $I = 16\hbar$, where the band terminates.

Both $\mathcal{J}_{\mathrm{TV}}(I)$ and $\mathcal{J}_{\mathrm{Ing}}(I)$ depend on the matrix elements of $\hat{J}_x$, as well as on the single-particle Routhians. The former, however, further takes into account the two-body residual interaction, whereas the latter does not. From this, we can infer that the two-body residual interaction plays a crucial role in reproducing the backbending phenomenon in the yrast band of ^{48}Cr. The particle alignment in this case is generated not by the one-body Coriolis term alone, but also by the nonlinear effects from the residual two-body interaction. This interaction contributes to the generation of a self-consistent mean field that accommodates a special occupied orbit with a property such that it easily aligns toward the direction of the total angular momentum.

One may thus reach another important conclusion, namely, that a self-consistent treatment of the two-body residual interaction at I is of special importance in reproducing the backbending phenomena where no level crossing of the single-particle orbits is observed. Thus, a theoretical analysis that uses the Inglis formula or a nonfully self-consistent mean-field theory such as the cranked Nilsson-Strutinsky method is not sufficient for an understanding of backbending phenomena in general.

ACKNOWLEDGMENTS

We are grateful to Professor Marumori for valuable discussions. One of the authors (T.T.) is also grateful to Professor Akaishi for his kind support, and to Professor Sawada and Dr. Sano for their hospitality.

[1] J. A. Cameron *et al.*, Phys. Lett. B **387**, 266 (1996).
[2] E. Caurier, J. L. Egido, G. Martínez-Pinedo, A. Poves, J. Retamosa, L. M. Robledo, and A. P. Zuker, Phys. Rev. Lett. **75**, 2466 (1995).
[3] I. Hamamoto, Nucl. Phys. **A271**, 15 (1976).
[4] K. Iwasawa, F. Sakata, Y. Hashimoto, and J. Terasaki, Prog. Theor. Phys. **92**, 1119 (1994); K. Iwasawa, F. Sakata, T. Tanaka, Y. Hashimoto, and T. Marumori, *Progress in Particle and Nuclear Physics* (Elsevier, New York, 1997), Vol. 38, p. 249.
[5] T. Marumori, F. Sakata, T. Une, T. Tanaka, and A. Onoda, Prog. Theor. Phys. **93**, 335 (1995).
[6] E. R. Marshalek and J. Weneser, Ann. Phys. (N.Y.) **53**, 569 (1969).
[7] D. M. Brink, M. J. Giannoni, and M. Veneroni, Nucl. Phys. **A258**, 237 (1976).
[8] A. K. Kerman and S. E. Koonin, Ann. Phys. (N.Y.) **100**, 332 (1976).
[9] F. Villars, Nucl. Phys. **A285**, 269 (1977).
[10] K. Goeke and P.-G. Reinhard, Ann. Phys. (N.Y.) **112**, 328 (1978).
[11] F. Sakata, T. Marumori, Y. Hashimoto, and T. Une, Prog. Theor. Phys. **70**, 424 (1983).
[12] F. Sakata, T. Kubo, T. Marumori, K. Iwasawa, and Y. Hash-

imoto, Phys. Rev. C **50**, 138 (1994).
[13] D. Gogny, *Nuclear Self-consistent Fields*, edited by G. Ripka and M. Porneuf (North-Holland, Amsterdam, 1973), p. 333.
[14] J. Decharge and D. Gogny, Phys. Rev. C **21**, 1568 (1980).
[15] M. Girod and B. Grammaticos, Phys. Rev. C **27**, 2317 (1983).
[16] T. Tanaka, F. Sakata, T. Marumori, and K. Iwasawa, Phys. Rev. C **56**, 180 (1997).
[17] E. R. Marshalek and A. L. Goodman, Nucl. Phys. **A294**, 92 (1978).
[18] R. A. Sorensen, Nucl. Phys. **A269**, 301 (1976).
[19] G. Audi and A. H. Wapstra, Nucl. Phys. **A565**, 1 (1993).